Contact resistivity of the p-type amorphous silicon hole contact in silicon heterojunction solar cells

Mehdi (Ashling) Leilaeioun*, William Weigand*, Mathieu Boccard, Zhengshan J. Yu, Kathryn Fisher, and Zachary C. Holman

***Abstract*—In silicon heterojunction solar cells made with high-lifetime wafers, resistive losses in the contacts dominate the total electrical power loss. Moreover, it is widely believed that the hole contact stack—a-Si:H(i)/a-Si:H(p)/ITO/Ag—is responsible for more of this power loss than the electron contact stack. In this paper, we vary the a-Si:H(i) layer thickness, the a-Si:H(p) layer thickness and doping, and the indium tin oxide (ITO) doping and determine the effect of each variation on the contact resistivity of the hole contact stack. In addition, we make complete solar cells with the same variations and correlate their series resistivity to the hole contact resistivity. We find that the contact resistivity is most sensitive to the thickness of the a-Si:H(i) layer and the oxygen partial pressure during ITO sputtering. Increasing the former from 4 to 16 nm results in a four-fold increase in contact resistivity, whereas increasing the latter from 0.14 to 0.85 mTorr raises the contact resistivity almost 30-fold. Optimized conditions produce a contact resistivity of 0.10 Ωcm^2 while maintaining an implied open-circuit voltage of 720 mV measured on cell precursors, which is the lowest contact resistivity value reported in the literature for an a-Si:H hole contact.**

***Index Terms*—Amorphous silicon, carrier-selective contact, contact resistivity, passivating contact, silicon heterojunction, solar cell.**

I. Introduction

P-type and n-type monocrystalline silicon wafers are now available with bulk lifetimes of greater than 1 ms [1, 2], and p-type multicrystalline silicon wafers now reach lifetimes of approximately 200 μs after a firing or phosphorous gettering process [3-5]. With these advances, the largest impediment to high solar cell efficiencies has shifted from recombination losses in the absorber to recombination and resistive losses in the contacts. Recent research efforts have thus aimed to develop contacts for which—in the case of a hole contact—the voltage drop produced by the hole current across the hole contact is less than a few millivolts and the electron current towards the hole contact is negligible. As described by Wurfel et al., the former ensures a high fill factor (*FF*) and the latter ensures a high open-circuit voltage (V_{oc}) [6].

These conditions are realized when, as described by Cuevas et al., the contact is selective: it has a large asymmetry in the conductivities of the two carrier types, with a high conductivity for holes (in the case of a hole contact) [7]. Brendel and Peibst represented selectivity, *S*, in terms of experimentally measureable parameters:

$$S = \frac{v_{th}}{J_{0c}\,\rho_c}$$

with v_{th} the thermal voltage, J_{0c} the contact recombination parameter, and ρ_c the contact resistivity [8]. J_{0c} captures the conductivity of electrons to a hole contact (or, more generally, the minority carrier with respect to the contact polarity) and can be determined through lifetime measurements [9], while ρ_c captures the conductivity of holes (or, more generally, the majority carrier with respect to the contact polarity) and can be determined via transfer length method (TLM) measurements [10], circular transfer length method (CTLM) measurements [11], or the through-the-absorber measurement introduced by Cox and Strack [12].

In their early work, Schroeder and Meier calculated that, for a silicon solar cell with a front contact area fraction of 5% and a front sheet resistance of 100 Ω/□, ρ_c must be less than 2 mΩcm^2 to keep the total power loss less than 0.5% [13]. For a contact that is full area, such as either contact in a typical amorphous silicon/crystalline silicon heterojunction (SHJ) solar cell, the conditions are more relaxed, allowing ρ_c as high as 83 mΩcm^2 for the same power loss. While one might expect that a 20-fold increase in contact area would result in a 20-fold increase in allowable contact resistivity, current crowding becomes important for smaller contact fractions, distorting the expected proportionality.

Table I provides a non-exhaustive list of different contacts, both metal-to-diffused-emitter stacks and multi-layer heterojunction stacks, and their reported respective contact resistivities. Although heterocontacts tend to have lower J_{0c} values than direct metal contacts, their corresponding ρ_c values

*A. Leilaeioun and W. Weigand contributed equally to this work.

This material is based upon work primarily supported by the Engineering Research Center Program of the National Science Foundation and the Office of Energy Efficiency and Renewable Energy of the Department of Energy under NSF Cooperative Agreement No. EEC-1041895. (Corresponding author: Zachary Holman)

A. Leilaeioun, Z.J. Yu, K. Fisher, and Z.C. Holman are with the School of Electrical, Computer and Energy Engineering at Arizona State University, Tempe, AZ 85287 (email: mehdi.leilaeioun@asu.edu; zhengshan.j.yu@asu.edu; kathryn.fisher@asu.edu; zachary.holman@asu.edu).

W. Weigand is with the School for Engineering of Matter, Transport and Energy at Arizona State University, Tempe, AZ 85287 (e-mail: william.weigand@asu.edu).

M. Boccard was with the School of Electrical, Computer and Energy Engineering at Arizona State University, Tempe, AZ 85287, and is presently with the Photovoltaics and Thin-Film Electronics Laboratory, Institute of Microengineering, Ecole Polytechnique Federale de Lausanne, Neuchatel CH-2002, Switzerland (email: mathieu.boccard@epfl.ch).

TABLE I
CONTACT RESISTIVITIES OF SELECT CONTACTS

Contact type	Contact test structure	ρ_c (m Ω cm^2)	Measurement technique
Metal to diffused emitter	c-Si(p)/c-Si(n$^+$)/Ag paste [21]	1 – 2	TLM
	c-Si(p)/c-Si(n$^+$)/Ni/Cu [22]	0.035	TLM
	c-Si(p)/c-Si(n$^+$)/Ti/Pd/Ag [22]	0.073	TLM
Electron heterocontact	Al/Mg/c-Si(n)/MgO$_x$/Al [23]	17.5	Cox and Strack
	c-Si(n)/a-Si:H(i)/Mg/Al [24]	310 (w/ a-Si:H layer)	Cox and Strack
		220 (w/o a-Si:H layer)	
	c-Si(n)/TiO$_x$/Ca/Al [25]	5	Cox and Strack
	c-Si(n)/LiF$_x$/Al [26]	2	TLM
	c-Si(n)/a-Si:H(i)/a-Si:H(n)/TCO/Metal [16]	370	Indirect
	c-Si(n)/a-Si:H(i)/a-Si:H(n)/Ti/Al [27]	30	CTLM
	c-Si(n)/a-Si:H(i)/a-Si:H(n)/Ti/Cu [27]	10	CTLM
	c-Si(n)/a-Si:H(i)/a-Si:H(n)/Ti/Pd/Ag [27]	10	CTLM
	c-Si(n)/a-Si:H(i)/a-Si:H(n)/Al [27]	10	CTLM
	c-Si(n)/a-Si:H(i)/μc-Si:H(n)/ITO/Ag [28]	47 (10˚C)	TLM
		36 (80˚C)	
	c-Si(n)/a-Si:H(i)/a-Si:H(n)/ITO/Ag [28]	448 (10˚C)	TLM
		55 (80˚C)	
	c-Si(n)/a-Si:H(i)/a-Si:H(n)/ITO/Ag [19]	140	TLM
	c-Si(n)/a-Si:H(i)/BZO/Ag [29]	40	TLM
	c-Si(n)/a-Si:H(i)/TiO$_x$/LiF/Al [30]	70	TLM
	c-Si(n)/LiF/Al [31]	26	TLM
Hole heterocontact	c-Si(p)/MoO$_x$/Pd/Al [32]	1 (p substrate)	Cox and Strack
		0.2 (p$^+$ substrate)	TLM
	c-Si(p)/a-Si:H(i)/μc-Si:H(p)/ITO/Ag [28]	600 (10˚C)	TLM
		170 (80˚C)	
	c-Si(p)/a-Si:H(i)/a-Si:H(p)/ITO/Ag [28]	1355 (10˚C)	TLM
		207 (80˚C)	
	c-Si(p)/a-Si:H(i)/a-Si:H(p)/TCO/Metal [16]	380	Indirect
	c-Si(p)/a-Si:H(i)/a-Si:H(p)/ITO/Ag [19]	240	TLM
	c-Si(p)/CuO$_x$:N/Pd/Ag [33, 34]	11	Cox and Strack
	Glass/PEDOT:PSS/Ag [35]	28	TLM
		790	

are 1–5 orders of magnitude higher, with the exception of the TiO$_x$/Ca/Al and LiF$_x$/Al electron contacts and the MoO$_x$/Pd/Al hole contact.

Interestingly, there are few reports analyzing the contact resistivity of SHJ heterocontacts, though they have been used to make silicon solar cells with efficiencies greater than 26% [14]. Gogolin et al. measured each of the resistive losses in SHJ cells except the contact resistance, and, by subtracting these from the total measured cell series resistance, determined that carrier transport through the amorphous silicon (a-Si:H) and across its interface with indium tin oxide (ITO) is responsible for the largest resistive loss [15]. Similarly, Lee et al. attempted to understand the resistive losses in SHJ contacts by creating test structures with one heterocontact and one Ohmic contact. The authors then subtracted the known component resistances, determined through similar test structures, from the total measured resistance. As seen in Table I, they obtained values of 0.38 and 0.37 Ωcm^2 for the c-Si(n)/a-Si:H(i)/a-Si:H(n)/ITO/Ag and c-Si(p)/a-Si:H(i)/a-Si:H(p)/ITO/Ag contacts, respectively, contradicting the notion that the hole contact—because of its position sandwiched between two low-work-function n-type materials—is the most detrimental in SHJ cells [16-18].

The most direct measurement of contact resistivities in SHJ solar cells came from Lachenal et al. [19]. Using TLM, these authors measured ρ_c = 0.14 and ρ_c = 0.24 Ωcm^2 for electron and hole SHJ contacts, respectively, that were nominally the same as those investigated by Lee et al. Together, these accounted for just over 60% of the total series resistivity (0.62 Ωcm^2) of a rear-emitter bifacial SHJ solar cell employing these contacts, as measured with the Suns-V$_{oc}$ technique [20].

In this paper, we extend the analysis of Lachenal et al. by measuring the contact resistivity as a function of the a-Si:H and ITO layer parameters, and by correlating the resistivities with cell performance. Specifically, we quantify the contact resistivity of an a-Si:H(i)/a-Si:H(p)/ITO/Ag hole contact in SHJ cells through TLM and Suns-V$_{oc}$ measurements. We do this analysis as a function of the a-Si:H(i) thickness, the a-Si:H(p) thickness and doping gas flow during plasma-enhanced vapor deposition (PECVD), and the oxygen gas partial pressure during ITO sputtering. The results reveal the processing parameters to which SHJ cell series resistance is most sensitive.

II. MATERIALS AND METHODS

We made TLM structures to measure contact resistivity, and we made complementary SHJ cells to extract pseudo fill factor (*pFF*), *FF*, and series resistivity (R_s). As shown in Figure 1a, the TLM structures consisted of a p-type wafer, a symmetric full-area a-Si:H(i)/a-Si:H(p) stack, and an ITO/Ag TLM

pattern. As shown in Figure 1b, the cells consisted of an n-type wafer with the same rear hole contact as used for the TLM structures, but with full-area ITO and Ag layers, and with a front electron heterocontact.

Boron- and phosphorous-doped Czochralski silicon wafers (156 mm pseudo-square) with resistivities of approximately 2 and 3.8 Ωcm, respectively, were double-side textured in potassium hydroxide to a thickness of 180 µm. The wafers were subsequently cleaned in RCA-B solution for metals removal,

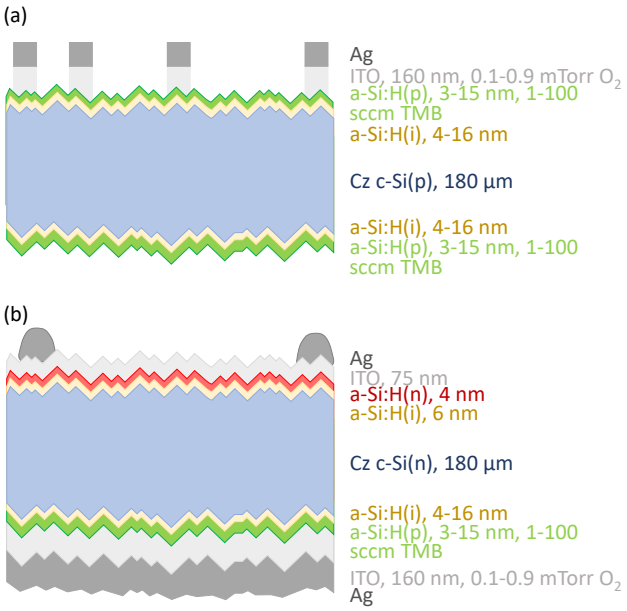

Fig. 1. Schematics of (a) TLM structures used to extract contact resistivity and (b) complete solar cells used to measure series resistivity.

Piranha solution for organics removal, and again in RCA-B solution for residual metals removal. They were then dipped in a 1:10 buffered oxide etch (BOE) solution for 1 minute to remove the native oxide on the surface, and subsequently put under vacuum for a-Si:H deposition.

The a-Si:H layers were deposited using radio frequency (RF,

TABLE II
GAS FLOW AND THICKNESSES FOR STANDARD A-SI:H LAYERS

	a-Si:H(i)	a-Si:H(p)	a-Si:H(n)
SiH_4 (sccm)	40	40	40
H_2 (sccm)	200	175	197
3% TMB (sccm)	–	18	–
1% PH_3 (sccm)	–	–	30
Thickness (nm)	6	11	5

13.56 MHz) PECVD in an Applied Materials P5000 tool. In any given experiment, a single parameter of one layer was varied and "standard" recipes were used for all other layers. Table II specifies the gas flow and thickness for the standard a-Si:H layers on textured wafers. Thickness measurements were performed on polished witness wafers and corrected for the additional area of textured surfaces. Note that for all recipes the chamber pressure was between 2 and 4 Torr and the substrate temperature was 250 °C. For the a-Si:H(i) thickness series, the deposition time was altered to achieve layers with thicknesses of 4 to 16 nm. For the a-Si:H(p) thickness series, the deposition time was altered to achieve layers with thicknesses of 3 to 13 nm. For the a-Si:H(p) gas flow series, the 3% trimethylborane (TMB) in hydrogen flow was varied from 1 to 100 sccm (126 to 8900 ppm of pure TMB); all concentrations reported hereafter are for pure TMB.

ITO layers were sputtered in an MRC 944 tool using a DC source power of 1 kW and a 90/10 In_2O_3/SnO_2 target. For the standard recipe, the chamber pressure was 7.1 mTorr with an oxygen partial pressure of 0.36 mTorr (all other gas was argon), and the thickness of the ITO layer in contact with the a-Si:H(p) layer was 160 nm on the textured surface. For the ITO oxygen concentration series, the oxygen flow was altered to arrive at oxygen partial pressures of 0.14 to 0.85 mTorr.

For the TLM structures, ITO and silver were sputtered through the same shadow mask without breaking vacuum to create TLM pads with spacings of 0.25 to 8 mm. The width of the pads was 2 mm and their length was 8 mm. After depositing the TLM pads, the wafers were annealed at 200 °C for 20 minutes to simulate the curing process of the low-temperature silver paste in full cells. Three TLM patterns were then cleaved from each wafer with a diamond-tipped pen, with the dimensions of the cleaved wafer sections as similar as possible to the dimensions of the overall TLM patterns. In initial TLM measurements, we performed a current-voltage sweep across each set of contacts using four probes. To make the measurements quicker, we switched to measuring resistance on a digital multimeter with two probes after confirming that this method reproduced the results from the four-probe method. The plots of resistance versus pad spacing were linear for all data presented in this work. The reported contact resistivity values are average values from the three TLM patterns cleaved from the same wafer, and error bars represent the standard deviation.

For the SHJ solar cells, the 75-nm-thick front ITO layer was sputtered through a shadow mask to define several 4 cm^2 cells per wafer, and low-temperature silver paste was screen-printed to form electrode grids. Full-area ITO and silver layers were sputtered on the rear of the wafer to form the rear electrode. The cells were then annealed at 200 °C for 20 minutes to cure the silver paste. A Sinton FCT-450 flash tester was used to measure the current-voltage and Suns-V_{oc} curves of each cell; these measurements used four probes and a 4 cm^2 illumination mask. From these measurements, we calculated R_s by comparing the Suns-V_{oc} curve with the current-voltage curve, as described by Sinton and Cuevas and elaborated by Pysch and Glunz [20, 36]. The reported *FF*, *pFF*, and R_s values are average values from three cells on the same wafer, and error bars represent the standard deviation.

III. RESULTS AND DISCUSSION

A. *a-Si:H(i) layer thickness*

Figure 2a shows that the SHJ cells studied here suffer from decreasing *FF* with a-Si:H(i) thickness beyond 4 nm, and Figures 2a and 2b reveal why: Although *pFF* improves by 1% absolute with the improved surface passivation, this is more than offset by the more than doubling of R_s from 1.19 to 2.75 Ωcm^2. Tanaka et al. similarly found that inserting a 4-nm-thick a-Si:H(i) layer between the c-Si wafer and a-Si:H(p) layer reduced surface recombination and resulted in an increase in *FF*

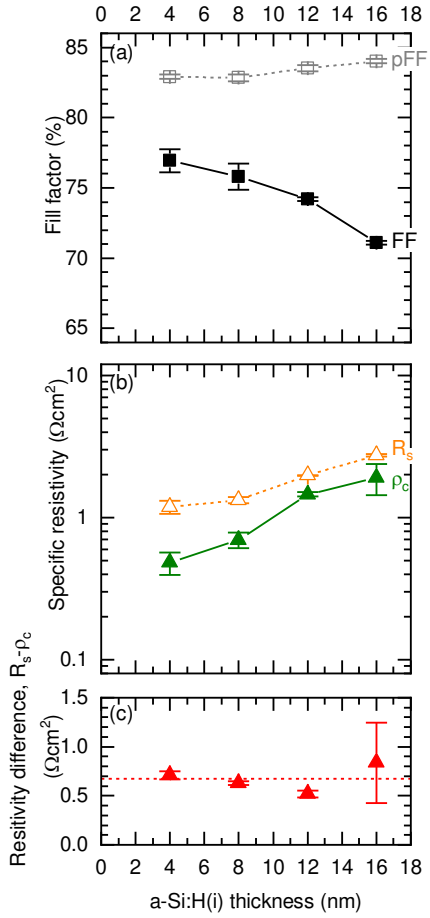

Fig. 2. SHJ solar cells and TLM structures with varying a-Si:H(i) layer thickness. (a) *pFF* and *FF*, (b) R_s and ρ_c, and (c) difference between R_s and ρ_c. The red dashed line is the average resistivity difference of all samples.

of approximately 0.8%, whereas further increases in the thickness caused *FF* to drop [37]. Holman et al. and Fujiwara and Kondo also found that a 4-nm-thick a-Si:H(i) layer produced the optimal cell efficiency, but these authors did not observe the same decreasing *FF* trend above this thickness [38, 39].

The increase in series resistivity in Figure 2b is entirely attributable to the contact resistivity of the hole contact, which rises from 0.48 to 1.91 Ωcm^2 over this a-Si:H(i) thickness range. This is apparent from Figure 2c, which shows that R_s–ρ_c remains constant. (Note that this difference remains between 0.5 and 0.7 Ωcm^2 for all experiments in this study, indicating the consistency of all sources of series resistance besides the hole contact stack.) The contact resistivity for the thinnest a-Si:H(i) layer is twice that reported by Lachenal et al. [19] and approximately 1.2 times that reported by Lee et al. [16]. However, not shown in this plot are results from a duplicate TLM experiment (but without complementary solar cells) performed several weeks later that yielded the same contact resistivity trend as in Figure 2b but with all values lower by approximately 0.3 Ωcm^2. The sample in that set with a 6-nm-thick a-Si:H(i) had the same contact resistivity (0.23 Ωcm^2) as that measured by Lachenal et al., within experimental error. This variation between nominally identical experiments performed several months apart was an early confirmation of what SHJ researchers intrinsically know and what is borne out in this work: the performance of SHJ contacts is sensitive to many processing parameters, and intimate control of the deposited layers is critical to avoid swings in *FF* between cell batches. In this particular case, we hypothesize that the variation was caused by a variation in oxygen gas flow while sputtering ITO across the several-weeks gap; Section IIIC reveals the sensitivity of contact resistivity to this parameter.

A complete explanation of the trend presented here requires an analysis of conduction thorough the a-Si:H(i) layer, but the exact mechanism is still debated. Two important mechanisms that are commonly used to describe the transport are multi-tunneling capture-emission (MTCE) [40] and diffusive transport similar to in a homojunction solar cell [41]. By performing transient capacitance measurements for multiple a-Si:H(i) layer thicknesses, Page et al. showed that the dominant hole transport mechanism is field-driven MTCE [42], whereas Mikolasek et al. revealed that MTCE is important for layers less than 5 nm thick and its effect diminishes for thicker layers [43]. We expect that a tunneling-dominated current will lead to an exponential increase in the resistance with increased layer thickness, whereas a diffusion-dominated current will lead to a linear increase. There are insufficient data, however, to conclusively identify either mechanism in Figure 2.

B. a-Si:H(p) layer thickness and doping

Those studies that investigated the a-Si:H(i) layer thickness usually also investigated the a-Si:H(p) layer thickness, with varying results. Tanaka et al. reported a decrease in *FF* from 73% to 70% with an increase in a-Si:H(p) thickness from 9 to 40 nm for SHJ cells without an underlying a-Si:H(i) layer [37]. By contrast, in SHJ cells with a passivating a-Si:H(i) layer, Fujiwara and Kondo found that the *FF* remained relatively constant as a function of a-Si:H(p) layer thickness when the thickness exceeded 3 nm, below which the *FF* sharply decreased [38]. And Holman et al. found a different behavior yet, with *FF* increasing for thicknesses greater than the 3 nm threshold determined by Fujiwara and Kondo [39].

A possible explanation for these discrepancies is variations in the doping density of the a-Si:H(p) layer, which was not reported by the authors. Bivour et al. demonstrated a 3% absolute increase in *FF* when the diborane doping gas concentration during a-Si:H(p) deposition was increased from 1400 ppm to 4300 ppm (10-nm-thick a-Si:H(p) layer), revealing the importance of this parameter [44]. In subsequent simulations, the same authors predicted increasing *FF* for increasing a-Si:H(p) layer thicknesses up to 4 nm, followed by constant *FF* of approximately 84% for thicker layers, in agreement with Fujiwara and Kondo [38]. This was true only for a highly doped a-Si:H(p) layer with an assumed activation energy of 0.2 eV, however; for an activation energy of 0.4 eV, which represents quite light doping, the simulated *FF* decreased with a-Si:H(p) thickness to below 70%.

Figure 3a shows that, in the cells fabricated here (which have the a-Si:H(p) layer on the rear, unlike in the aforementioned studies), the *pFF* remains constant, within experimental error, at 81.5% over the entire thickness range. Similar to Fujiwara and Kondo, the *FF* also remains relatively constant at approximately 78% for a-Si:H(p) layer thicknesses of 6 nm and greater, but drops to 76% for 3 nm. Figure 3b indicates that, as

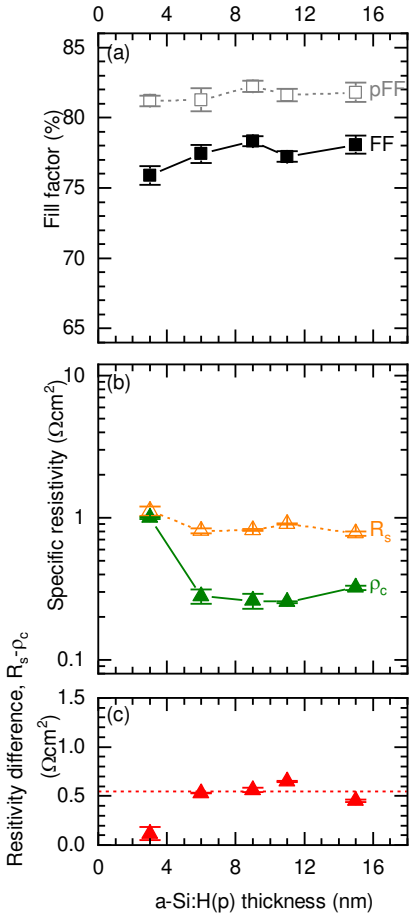

Fig. 3. SHJ solar cells and TLM structures with varying a-Si:H(p) layer thickness. (a) *pFF* and *FF*, (b) R_s and ρ_c, and (c) difference between R_s and ρ_c. The red dashed line is the average resistivity difference of the three thickest samples.

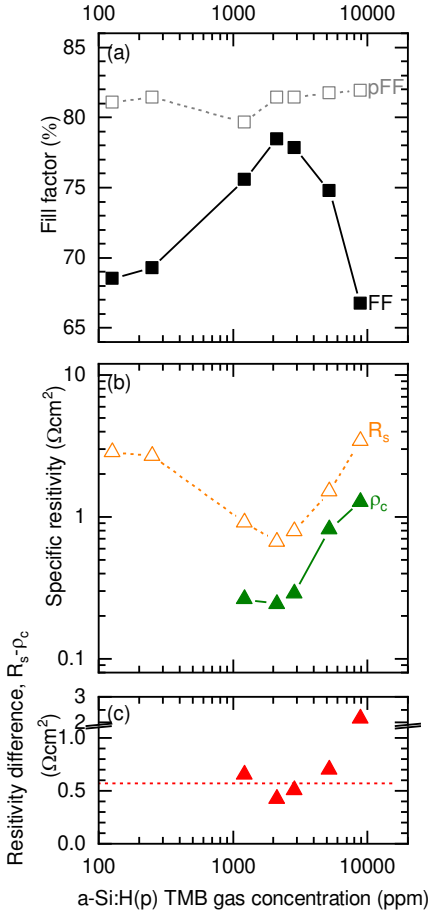

Fig. 4. SHJ solar cells and TLM structures with varying a-Si:H(p) TMB gas concentration. (a) *pFF* and *FF*, (b) R_s and ρ_c, and (c) difference between R_s and ρ_c. The red dashed line is the average resistivity difference of the four samples with the lowest concentration. Only one cell and TLM pad was measured for each condition in this experiment.

expected, R_s is constant for thicker layers, and that this occurs because ρ_c is constant. For the thinnest layer, however, ρ_c triples and the difference between R_s and ρ_c in Figure 3c becomes suspiciously small. We suspect that the poor performance of this cell is likely the result of the thin a-Si:H(p) layer being depleted by the adjacent ITO layer, which would increase its resistance to holes [45]. Kanevce and Metzger simulated a SHJ solar cell with an a-Si:H(p) doping of 3×10^{19} cm^{-3} and showed that a V_{oc} approaching 700 mV is possible only with a thickness greater than 7 nm; thinner layers face depletion [46]. Although it is challenging to measure the hole density of a-Si:H(p), our previous simulations indicated that a density of $1–2\times10^{19}$ cm^{-3}—corresponding to a reasonable dopant activation efficiency of approximately 1% [47], given a boron concentration of 9×10^{20} cm^{-3} measured by secondary-ion mass spectrometry—is consistent with our measured contact resistivity for our standard layer [48, 49], and a-Si:H(p) layers with this density should then be depleted if they are less than 7 nm thick.

Cells fabricated with (standard 11-nm-thick) a-Si:H(p) layers having varying doping density have approximately constant *pFF* of 81–82%, as seen in Figure 4a. The *FF* has quite a different trend: it increases up to a TMB gas concentration of 2117 ppm, while a subsequent increase in the TMB gas concentration leads to a peculiar decrease that is inconsistent with increasing hole density. Both R_s and ρ_c mirror the *FF* (Figure 4b), with a nearly constant offset between the two except for at the highest TMB gas concentration (Figure 4c), confirming that the large swings in cell performance are attributable to the varying resistance of the hole contact. We suspect that depletion of the a-Si:H(p) layer at low TMB gas concentration is again responsible for the high resistivities. Noting the layer's 11 nm thickness, we calculate that it should become depleted by the adjacent ITO for doping densities below 6×10^{18} cm^{-3}. Given our earlier estimated doping density of $1–2\times10^{19}$ cm^{-3} for our standard layer with a TMB concentration of 2117 ppm, and assuming slowly varying or unvarying dopant activation efficiency, this would mean that the a-Si:H(p) layer would become depleted for TMB concentrations below roughly 700–1400 ppm. Figure 4b indicates that this is the concentration range below which the contact and series resistivities rise, and thus the data is consistent with this depletion hypothesis.

For TMB gas concentrations greater than 2117 ppm, the increase in ρ_c may be caused by dopant-induced defect formation that occurs at a faster rate than active dopant formation [50]. In the dopant-induced defect regime, the hole density, $N_{hole} = N_{dopant} - N_{defect}$, shrinks. Pysch et al. reported that the decreased hole density becomes evident when

the diborane gas concentration exceeds 3,500 ppm, due to the increase in dangling-bond-like defects formed by heavy extrinsic doping [50]. Similarly, for the electron heterocontact, Korte et al. observed through constant-final-state yield spectroscopy that the Fermi level in a-Si:H(n) returns towards mid-gap when the phosphine gas concentration exceeds 20,000 ppm, indicating that at high enough dopant density the electron density decreases [51]. A reduction in the hole density would facilitate the depletion of the a-Si:H(p) layer—again—leading to an increase in the contact resistivity of the stack.

C. *ITO doping*

Much of the experimental work on transparent conductive oxide (TCO) layers for SHJ solar cells focused on sheet resistance, contact resistivity between the metal and TCO, and free-carrier absorption, without regard to the layers' role in the contact resistivity of the whole stack, and specifically its interaction with the underlying a-Si:H layers [39, 52, 53]. However, the growing gap between *pFF* and *FF* in Figure 5a with varying oxygen partial pressure during ITO deposition reveals that this layer can have a dramatic influence on contact resistance. (Recall that the varied ITO layer is at the back of the cell and thus the accompanying change in its sheet resistance is unimportant; this is confirmed by Figure 5c, which shows that the non-ρ_c contributions to R_s are nearly the same for all cells, with only a minimal increase that may be statistically significant.) Bivour et al. observed a similar *FF* trend with increasing oxygen concentration, but they did not study the corresponding effect on ρ_c [54]. Both R_s and ρ_c mirror the *FF*, with a nearly constant offset (Figure 5b and 5c), indicating that the drastic changes in device performance arise from changes in the hole contact resistivity. Note that the contact resistivity of 0.10 Ωcm^2 for the 0.14 mTorr sample is the lowest value that has been reported for the hole contact in SHJ solar cells. In fact, while the short-circuit current of these solar cells decreased slightly compared to the cells with higher oxygen partial pressure, the increase in *FF*, due to low ρ_c, provided a boost in efficiency (not shown).

Increasing oxygen partial pressure during sputtering fills oxygen vacancies, reducing the electron density and enlarging the ITO work function [55, 56]. In simulation studies, Centurioni and Iencinella showed a 30% drop in *FF* when the TCO work function decreased from 5.1 to 4.75 eV [57], contrary to the trend in Figure 5a. Similarly, Bivour et al. found that heavily and moderately doped a-Si:H(p) layers required minimum TCO work functions of 4.7 and 5 eV, respectively to obtain reasonable *FF* [18]. However, both studies treated the TCO as a metallic layer and not as an n-type semiconductor. Our recent simulations showed that, to accurately recreate measured contact resistance trends, the ITO must be modelled as a semiconductor because the heavily doped a-Si:H(p) and ITO form a tunnel junction [48]. One hypothesis that is consistent with Figure 5, posed by Bivour et al. [54], postulates that increasing work function misaligns the a-Si:H(p) valence band and the ITO conduction band, suppressing band-to-band tunneling across the interface [46]. This, in turn, increases the resistance of the contact and reduces *FF*. In fact, Kirner et al. previously simulated and experimentally verified that a decrease in ITO doping results in decreased *FF* with S-shaped

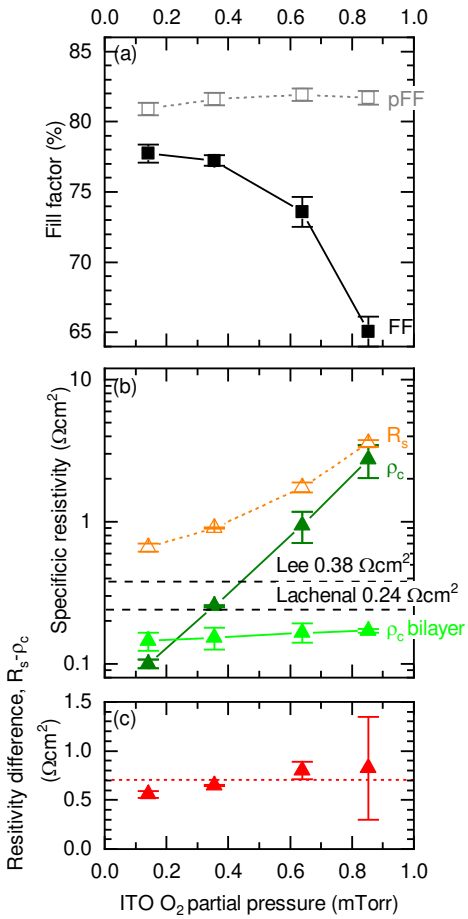

Fig. 5. SHJ solar cells and TLM structures with varying O_2 partial pressure during ITO sputtering. (a) *pFF* and *FF*, (b) R_s and ρ_c, and (c) difference between R_s and ρ_c. The black dashed lines indicate the values reported by Lee et al. and Lachenal et al. [16,19]. The red dashed line is the average resistivity difference of all samples.

current–voltage curves, and they attributed this to suppression of the tunneling current across the a-Si:H(p)/ITO interface [58].

To further investigate the role of the a-Si:H(p)/ITO interface in the high contact resistivities in Figure 5b, we made similar TLM structures with a bilayer of ITO consisting of a 15-nm-thick layer deposited with a low oxygen partial pressure of 0.14 mTorr and a subsequent, 145-nm-thick capping layer with oxygen partial pressures between 0.14 and 0.85 mTorr. As shown in Figure 5b, regardless of the capping layer oxygen

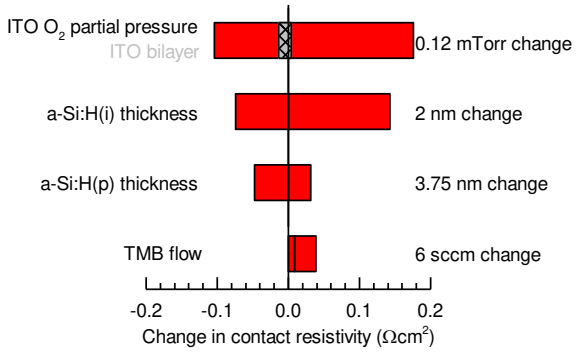

Fig. 6. Absolute change in contact resistivity as a function of the four parameters varied in this work. All variations are 33% of the standard process.

partial pressure, the contact resistivity of these samples was approximately 0.15 Ωcm^2, indicating the importance of band alignment, and not necessarily low ITO work function, for transport across the a-Si:H(p)/ITO interface. These bilayers are expected to combine low contact resistivity with high infrared transparency—due to the high oxygen-partial-pressure layer used for the capping layer, which accounts for most of the ITO thickness—and may provide a unique opportunity to increase the short-circuit current of the cell without compromising *FF*.

D. Processes that dominate contact resistivity

Figure 6 shows which processes in the fabrication of the hole contact for SHJ solar cells most strongly influence the contact resistivity. The changes correspond to 33% variations above and below our standard processes outlined in Section II. Perturbations of this magnitude are typical when exploring the deposition parameter space to find an optimal process from a current baseline process.

Although Figure 4 indicates that the TMB concentration can dramatically affect the contact resistivity, only an appreciable change from the standard process results in large excursions from the optimum value. Figure 6 thus reveals that the contact resistivity is least sensitive to TMB flow rate, of the parameters explored. In addition, unlike for the other parameters, variations from the optimal TMB concentration in either direction increase the contact resistivity, as our standard process lies at the minimum contact resistivity in Figure 4b.

The a-Si:H(p) layer thickness matters little unless the thickness drops below 3 nm (Figure 3) which is not seen in Figure 6 because this thickness is not within the 33% perturbation. However, in the case of a front-hole-contact device, the best efficiencies are achieved with thinner a-Si:H(p) layers due to the reduced parasitic absorption of visible light [39].

An increase in the a-Si:H(i) layer thickness of only 2 nm results in a contact resistivity increase of 0.14 Ωcm^2, and a decrease of 2 nm results in a decrease of 0.07 Ωcm^2. This may be significant for industrial PECVD systems where it is entirely possible to have a thickness variation of this magnitude across the chamber [59-61]. Because the change in contact resistivity is asymmetric with a-Si:H(i) thickness perturbation, it is wise—from a contact resistance perspective—to err on the side of too thin. This, however, can result in poorer passivation and thus a loss in V_{oc}.

The largest detriment to the contact resistivity comes from varying the ITO partial pressure, with a large change in ρ_c resulting from a change in the oxygen partial pressure of only 0.12 mTorr. Fortunately, for the sputtering tool used here, this variation corresponds to a 0.5 sccm change (out of 1.6 sccm) from the standard ITO oxygen gas flow. Although this is at the low end of the mass flow controller's range and drifts over time may exceed this value, flow variations within a given deposition are typically within 0.1 sccm. The ITO bilayer dampens the sensitivity of ρ_c to oxygen partial pressure and thus offers an alternative approach to widen the ITO process window.

IV. Conclusions

We have revealed that the contact resistivity of the hole contact in SHJ solar cells, and thus the cell *FF*, is most strongly affected by changes in the oxygen partial pressure during ITO sputtering (except when a bilayer is used) and in a-Si:H(i) layer thickness. These processes should be closely monitored to maintain consistently high-efficiency SHJ cells. Through careful process control, we achieved a minimum hole contact resistivity of 0.10 Ωcm^2. With unity contact fraction, this contact would cause near-negligible power loss in two-terminal tandem devices in which the current density is below 20 mA/cm^2, but it is still high enough to produce just over 0.5% power loss in single-junction silicon cells.

One approach to further reduce the contact resistivity is to undertake a theoretical and experimental analysis of the transport physics, which will provide insight into the limiting transport mechanisms. In particular, simulations that treat ITO as a semiconductor can bolster or disprove our hypothesis that tunneling due to proper band alignment at the a-Si:H(p)/ITO interface is more important than a high work function in determining contact resistivity. And, if the band-alignment hypothesis is confirmed, subsequent simulations can predict the contact resistivities with other TCO materials and hole-selective materials, after measuring their work function and electron affinity. Candidate TCO materials that may warrant study include boron-doped zinc oxide [62], with the favorable band alignment between its conduction band and the valence band of p-type microcrystalline silicon, and amorphous indium zinc oxide [63], for which cell *FF* trends are similar to those presented for our ITO, suggesting similar transport. Hole-selective materials to be further investigated include MoO_x [32] and $CuO:N_x$ [33, 64], both of which have a low contact resistivity to silicon with moderate surface passivation. Not to be forgotten, additional investigation into SHJ hole contacts and their resistivities should be accompanied by parallel investigation into SHJ electron contacts—which have not yet received the detailed resistivity analysis presented here—as further reduction in *FF* loss requires the minimization of both resistivities.

References

[1] J. E. Cotter, J. H. Guo, P. J. Cousins, M. D. Abbott, F. W. Chen, and K. C. Fisher, "P-Type Versus n-Type Silicon Wafers: Prospects for High-Efficiency Commercial Silicon Solar Cells," *IEEE Transactions on Electron Devices,* vol. 53, no. 8, pp. 1893-1901, 2006.

[2] D. C. Walter, B. Lim, K. Bothe, R. Falster, V. V. Voronkov, and J. Schmidt, "Lifetimes exceeding 1ms in 1-Ωcm boron-doped Cz-silicon," *Solar Energy Materials and Solar Cells,* vol. 131, pp. 51-57, 2014.

[3] A. Cuevas, M. Stocks, S. Armand, M. Stuckings, A. Blakers, and F. Ferrazza, "High minority carrier lifetime in phosphorus-gettered multicrystalline silicon," *Applied Physics Letters,* vol. 70, no. 8, pp. 1017-1019, 1997.

[4] S. A. McHugo, H. Hieslmair, and E. R. J. A. P. A. Weber, "Gettering of metallic impurities in photovoltaic silicon," journal article vol. 64, no. 2, pp. 127-137, January 01 1997.

[5] B. Vicari Stefani, W. Weigand, M. Wright, A. Soeriyadi, Z. Yu, M. Kim, D. Chen, Z. Holman, and B. Hallam, "P-type Upgraded Metallurgical-Grade Multicrystalline Silicon Heterojunction Solar Cells with Open-Circuit Voltages over 690 mV," *physica status solidi (a),* vol. 0, no. 0, p. 1900319, 2019/06/04 2019.

[6] U. Wurfel, A. Cuevas, and P. Wurfel, "Charge Carrier Separation in Solar Cells," *IEEE Journal of Photovoltaics,* vol. 5, no. 1, pp. 461-469, 2015.

[7] A. Cuevas, T. Allen, J. Bullock, W. Yimao, Di, and Z. Xinyu, "Skin care for healthy silicon solar cells," in *2015 IEEE 42nd Photovoltaic Specialist Conference (PVSC)*, 2015, pp. 1-6.

[8] R. Brendel and R. Peibst, "Contact Selectivity and Efficiency in Crystalline Silicon Photovoltaics," *IEEE Journal of Photovoltaics,* vol. 6, no. 6, pp. 1413-1420, 2016.

[9] A. Cuevas, R. A. Sinton, and M. Stuckings, "Determination of recombination parameters in semiconductors from photoconductance measurements," in *1996 Conference on Optoelectronic and Microelectronic Materials and Devices. Proceedings*, 1996, pp. 16-19.

[10] D. L. Meier and D. K. Schroder, "Contact resistance: Its measurement and relative importance to power loss in a solar cell," *IEEE Transactions on Electron Devices,* vol. 31, no. 5, pp. 647-653, 1984.

[11] G. S. Marlow and M. B. Das, "The effects of contact size and non-zero metal resistance on the determination of specific contact resistance," *Solid-State Electronics,* vol. 25, no. 2, pp. 91-94, 1982/02/01/ 1982.

[12] R. H. Cox and H. Strack, "Ohmic contacts for GaAs devices," *Solid-State Electronics,* vol. 10, no. 12, pp. 1213-1218, 1967/12/01/ 1967.

[13] D. K. Schroder and D. L. Meier, "Solar cell contact resistance—A review," *IEEE Transactions on Electron Devices,* vol. 31, no. 5, pp. 637-647, 1984.

[14] K. Yoshikawa, H. Kawasaki, W. Yoshida, T. Irie, K. Konishi, K. Nakano, T. Uto, D. Adachi, M. Kanematsu, H. Uzu, and K. Yamamoto, "Silicon heterojunction solar cell with interdigitated back contacts for a photoconversion efficiency over 26%," *Nature Energy,* Article vol. 2, p. 17032, 03/20/online 2017.

[15] R. Gogolin, M. Turcu, R. Ferre, J. Clemens, N.-P. Harder, R. Brendel, and J. Schmidt, "Analysis of Series Resistance Losses in a-Si:H/c-Si Heterojunction Solar Cells," *IEEE Journal of Photovoltaics,* vol. 4, no. 5, pp. 1169-1176, 2014.

[16] S.-Y. Lee, H. Choi, H. Li, K. Ji, S. Nam, J. Choi, S.-W. Ahn, H.-M. Lee, and B. Park, "Analysis of a-Si:H/TCO contact resistance for the Si heterojunction back-contact solar cell," *Solar Energy Materials and Solar Cells,* vol. 120, pp. 412-416, 2014.

[17] A. Kanevce and W. K. Metzger, "Device Physics of Heterojunction with Intrinsic Thin Layer (HIT) Solar Cells," *MRS Proceedings,* vol. 1153, pp. 1153-A10-04, 2009, Art no. 1153-a10-04.

[18] M. Bivour, S. Schröer, and M. Hermle, "Numerical analysis of electrical TCO / a-Si:H(p) contact properties for silicon heterojunction solar cells," *Energy Procedia,* vol. 38, pp. 658-669, 2013.

[19] D. Lachenal, D. Baetzner, W. Frammelsberger, B. Legradic, J. Meixenberger, P. Papet, B. Strahm, and G. Wahli, "Heterojunction and Passivated Contacts: A Simple Method to Extract Both n/tco and p/tco Contacts Resistivity," *Energy Procedia,* vol. 92, pp. 932-938, 2016.

[20] R. Sinton and A. Cuevas, "A quasi-steady-state open-circuit voltage method for solar cell characterization," *16th European Photovoltaic Solar Energy Conference,* pp. 1-4, 2000.

[21] M. M. Hilali, A. Rohatgi, and S. Asher, "Development of Screen-Printed Silicon Solar Cells With High Fill Factors on 100<tex>$Omega$</tex>/sq Emitters," *IEEE Transactions on Electron Devices,* vol. 51, no. 6, pp. 948-955, 2004.

[22] E. J. Lee, D. S. Kim, and S. H. Lee, "Ni/Cu metallization for low-cost high-efficiency PERC cells," *Solar Energy Materials and Solar Cells,* vol. 74, no. 1, pp. 65-70, 2002/10/01/ 2002.

[23] Y. Wan, C. Samundsett, J. Bullock, M. Hettick, T. Allen, D. Yan, J. Peng, Y. Wu, J. Cui, A. Javey, and A. Cuevas, "Conductive and Stable Magnesium Oxide Electron-Selective Contacts for Efficient Silicon Solar Cells," *Advanced Energy Materials,* vol. 7, no. 5, p. 1601863, 2017/03/01 2016.

[24] Y. Wan, C. Samundsett, D. Yan, T. Allen, J. Peng, J. Cui, X. Zhang, J. Bullock, and A. Cuevas, "A magnesium/amorphous silicon passivating contact for n-type crystalline silicon solar cells," *Applied Physics Letters,* vol. 109, no. 11, p. 113901, 2016.

[25] T. G. Allen, J. Bullock, Q. Jeangros, C. Samundsett, Y. Wan, J. Cui, A. Hessler-Wyser, S. De Wolf, A. Javey, and A. Cuevas, "A Low Resistance Calcium/Reduced Titania Passivated Contact for High Efficiency Crystalline Silicon Solar Cells," *Advanced Energy Materials,* vol. 7, no. 12, pp. 1602606-n/a, 2017, Art no. 1602606.

[26] J. Bullock, P. Zheng, Q. Jeangros, M. Tosun, M. Hettick, C. M. Sutter-Fella, Y. Wan, T. Allen, D. Yan, D. Macdonald, S. De Wolf, A. Hessler-Wyser, A. Cuevas, and A. Javey, "Lithium Fluoride Based Electron Contacts for High Efficiency n-Type Crystalline Silicon Solar Cells," *Advanced Energy Materials,* vol. 6, no. 14, pp. 1600241-n/a, 2016, Art no. 1600241.

[27] R. Labie, T. Bearda, O. El Daif, B. O'Sullivan, K. Baert, and I. Gordon, "Resistance and passivation of metal contacts using n-type amorphous Si for Si solar cells," *Journal of Applied Physics,* vol. 115, no. 18, 2014.

[28] G. Nogay, J. P. Seif, Y. Riesen, A. Tomasi, Q. Jeangros, N. Wyrsch, F. Haug, S. D. Wolf, and C. Ballif, "Nanocrystalline Silicon Carrier Collectors for Silicon Heterojunction Solar Cells and Impact on Low-Temperature Device Characteristics," *IEEE Journal of Photovoltaics,* vol. 6, no. 6, pp. 1654-1662, 2016.

[29] F. Wang, S. Zhao, B. Liu, Y. Li, Q. Ren, R. Du, N. Wang, C. Wei, X. Chen, G. Wang, B. Yan, Y. Zhao, and X. Zhang, "Silicon solar cells with bifacial metal oxides carrier selective layers," *Nano Energy,* vol. 39, pp. 437-443, 2017.

[30] J. Bullock, Y. Wan, Z. Xu, S. Essig, M. Hettick, H. Wang, W. Ji, M. Boccard, A. Cuevas, C. Ballif, and A. Javey, "Stable Dopant-Free Asymmetric Heterocontact Silicon Solar Cells with Efficiencies above 20%," *ACS Energy Letters,* vol. 3, no. 3, pp. 508-513, 2018/03/09 2018.

[31] Y. Zhang, R. Liu, S.-T. Lee, and B. Sun, "The role of a LiF layer on the performance of poly(3,4-ethylenedioxythiophene):poly(styrenesulfonate)/Si organic-inorganic hybrid solar cells," *Applied Physics Letters,* vol. 104, no. 8, 2014.

[32] J. Bullock, A. Cuevas, T. Allen, and C. Battaglia, "Molybdenum oxide MoOx: A versatile hole contact for silicon solar cells," *Applied Physics Letters,* vol. 105, 2014.

[33] X. Zhang, Y. Wan, J. Bullock, T. Allen, and A. Cuevas, "Low resistance Ohmic contact to p-type crystalline silicon via nitrogen-doped copper oxide films," *Applied Physics Letters,* vol. 109, 2016.

[34] X. Zhang, Y. Wan, J. Bullock, T. Allen, and A. Cuevas, "Low resistance Ohmic contact to p-type crystalline silicon via nitrogen-doped copper oxide films," *Applied Physics Letters,* vol. 109, no. 5, 2016.

[35] S. Mahato, L. G. Gerling, C. Voz, R. Alcubilla, and J. Puigdollers, "PEDOT:PSS as an Alternative Hole Selective Contact for ITO-Free Hybrid Crystalline Silicon Solar Cell," *IEEE Journal of Photovoltaics,* vol. 6, no. 4, pp. 934-939, 2016.

[36] D. Pysch, A. Mette, and S. W. Glunz, "A review and comparison of different methods to determine the series resistance of solar cells," (in English), *Solar Energy Materials and Solar Cells,* vol. 91, no. 18, pp. 1698-1706, Nov 6 2007.

[37] T. Makoto, T. Mikio, M. Takao, S. Toru, T. Shinya, N. Shoichi, H. Hiroshi, and K. Yukinori, "Development of New a-Si/c-Si Heterojunction Solar Cells: ACJ-HIT (Artificially Constructed Junction-Heterojunction with Intrinsic Thin-Layer)," *Japanese Journal of Applied Physics,* vol. 31, no. 11R, p. 3518, 1992.

[38] H. Fujiwara and M. Kondo, "Effects of a-Si:H layer thicknesses on the performance of a-Si:H/c-Si heterojunction solar cells," *Journal of Applied Physics,* vol. 101, no. 5, 2007.

[39] Z. C. Holman, A. Descoeudres, L. Barraud, F. Z. Fernandez, J. P. Seif, S. De Wolf, and C. Ballif, "Current Losses at the Front of Silicon Heterojunction Solar Cells," *IEEE Journal of Photovoltaics,* vol. 2, no. 1, pp. 7-15, 2012.

[40] H. Matsuura, T. Okuno, H. Okushi, and K. Tanaka, "Electrical properties ofn-amorphous/p-crystalline silicon heterojunctions," *Journal of Applied Physics,* vol. 55, no. 4, pp. 1012-1019, 1984.

[41] T. Mikio, M. Eiji, and T. Makoto, "Temperature Dependence of Amorphous/Crystalline Silicon Heterojunction Solar Cells," *Japanese Journal of Applied Physics,* vol. 47, no. 2R, p. 814, 2008.

[42] M. R. Page, E. Iwaniczko, Y. Q. Xu, L. Roybal, F. Hasoon, Q. Wang, and R. S. Crandall, "Amorphous/crystalline silicon heterojunction solar cells with varying i-layer thickness," *Thin Solid Films,* vol. 519, no. 14, pp. 4527-4530, May 2011.

[43] M. Mikolášek, M. Nemec, M. Vojs, J. Jakabovič, V. Řeháček, D. Zhang, M. Zeman, and L. Harmatha, "Electrical transport mechanisms in amorphous/crystalline silicon heterojunction: Impact of passivation layer thickness," *Thin Solid Films,* vol. 558, pp. 315-319, 2014/05/02/ 2014.

[44] M. Bivour, C. Reichel, M. Hermle, and S. W. Glunz, "Improving the a-Si:H(p) rear emitter contact of n-type silicon solar cells," *Solar Energy Materials and Solar Cells,* vol. 106, pp. 11-16, 2012.

[45] H. Schade and Z. E. Smith, "Contact resistance measurements for hydrogenated amorphous silicon solar cell structures," *Journal of Applied Physics,* vol. 59, no. 5, pp. 1682-1687, 1986.

[46] A. Kanevce and W. K. Metzger, "The role of amorphous silicon and tunneling in heterojunction with intrinsic thin layer (HIT) solar cells," *Journal of Applied Physics,* vol. 105, no. 9, p. 094507, 2009/05/01 2009.

[47] R. A. Street, "Doping and the fermi energy in amorphous silicon," *Physical Review Letters,* vol. 49, pp. 1187-1190, 1982.

[48] M. Leilaeioun, W. Weigand, P. Muralidharan, M. Boccard, D. Vasileska, S. Goodnick, and Z. Holman, "TLM measurements varying the intrinsic a-Si:H layer thickness in silicon heterojunction solar cells," in *2017 IEEE 44th Photovoltaic Specialist Conference (PVSC)*, 2017, pp. 1790-1793.

[49] P. Muralidharan, A. M. Leilaeioun, W. Weigand, Z. C. Holman, S. M. Goodnick, and D. Vasileska, "Understanding Transport in Heterojunction Contact Stacks by Simulating Silicon Heterojunction TLM Structures," in *2018 IEEE 7th World Conference on Photovoltaic Energy Conversion (WCPEC) (A Joint Conference of 45th IEEE PVSC, 28th PVSEC & 34th EU PVSEC)*, 2018, pp. 2166-2169.

[50] D. Pysch, C. Meinhard, N.-P. Harder, M. Hermle, and S. W. Glunz, "Analysis and optimization approach for the doped amorphous layers of silicon heterojunction solar cells," *Journal of Applied Physics,* vol. 110, no. 9, 2011.

[51] L. Korte, E. Conrad, H. Angermann, R. Stangl, and M. Schmidt, "Advances in a-Si:H/c-Si heterojunction solar cell fabrication and characterization," *Solar Energy Materials and Solar Cells,* vol. 93, no. 6, pp. 905-910, 2009/06/01/ 2009.

[52] Z. C. Holman, M. Filipič, A. Descoeudres, S. De Wolf, F. Smole, M. Topič, and C. Ballif, "Infrared light management in high-efficiency silicon heterojunction and rear-passivated solar cells," *Journal of Applied Physics,* vol. 113, no. 1, 2013.

[53] M. Balestrieri, D. Pysch, J. P. Becker, M. Hermle, W. Warta, and S. W. Glunz, "Characterization and optimization of indium tin oxide films for heterojunction solar cells," *Solar Energy Materials and Solar Cells,* vol. 95, no. 8, pp. 2390-2399, 2011/08/01/ 2011.

[54] M. Bivour, M. Reusch, F. Feldmann, M. Hermle, and S. Glunz, *Requirements for Carrier Selective Silicon Heterojunctions*. 2014.

[55] M. Balestrieri, D. Pysch, J. P. Becker, M. Hermle, W. Warta, and S. W. Glunz, "Characterization and optimization of indium tin oxide films for heterojunction solar cells," *Solar Energy Materials and Solar Cells,* vol. 95, pp. 2390-2399, 2011.

[56] S. Li, X. Qiao, and J. Chen, "Effects of oxygen flow on the properties of indium tin oxide films," *Materials Chemistry and Physics,* vol. 98, no. 1, pp. 144-147, 2006/07/01/ 2006.

[57] E. Centurioni and D. Iencinella, "Role of front contact work function on amorphous silicon/crystalline silicon heterojunction solar cell performance," (in English), *Ieee Electr Device L,* vol. 24, no. 3, pp. 177-179, Mar 2003.

[58] S. Kirner, M. Hartig, L. Mazzarella, L. Korte, T. Frijnts, H. Scherg-Kurmes, S. Ring, B. Stannowski, B. Rech, and R. Schlatmann, "The Influence of ITO Dopant Density on J-V Characteristics of Silicon Heterojunction Solar Cells: Experiments and Simulations," *Energy Procedia,* vol. 77, pp. 725-732, 2015/08/01/ 2015.

[59] A. A. Howling, L. Sansonnens, J. Ballutaud, C. Hollenstein, and J. P. M. Schmitt, "Nonuniform radio-frequency plasma potential due to edge asymmetry in large-area radio-frequency reactors," *Journal of Applied Physics,* vol. 96, no. 10, pp. 5429-5440, 2004.

[60] H. Takatsuka, Y. Yamauchi, K. Kawamura, H. Mashima, and Y. Takeuchi, "World's largest amorphous silicon photovoltaic module," *Thin Solid Films,* vol. 506-507, pp. 13-16, 2006.

[61] B. Legradic, B. Strahm, D. Lachenal, D. Bätzner, W. Frammelsberger, J. Meixenberger, P. Papet, G. Wahli, Z. Jun, D. Decker, and E. Vetter, "High efficiency Si-heterojunction technology - it's ready for mass production," in *2015 IEEE 42nd Photovoltaic Specialist Conference (PVSC)*, 2015, pp. 1-3.

[62] D. Gerlach, R. G. Wilks, D. Wippler, M. Wimmer, M. Lozac'h, R. Félix, A. Mück, M. Meier, S. Ueda, H. Yoshikawa, M. Gorgoi, K. Lips, B. Rech, M. Sumiya, J. Hüpkes, K. Kobayashi, and M. Bär, "The silicon/zinc oxide interface in amorphous silicon-based thin-film solar cells: Understanding an empirically optimized contact," *Applied Physics Letters,* vol. 103, no. 2, p. 023903, 2013/07/08 2013.

[63] M. Morales-Masis, S. M. D. Nicolas, J. Holovsky, S. D. Wolf, and C. Ballif, "Low-Temperature High-Mobility Amorphous IZO for Silicon Heterojunction Solar Cells," *IEEE Journal of Photovoltaics,* vol. 5, no. 5, pp. 1340-1347, 2015.

[64] P. Ravindra, R. Mukherjee, and S. Avasthi, "Hole-Selective Electron-Blocking Copper Oxide Contact for Silicon Solar Cells," *IEEE Journal of Photovoltaics,* vol. 7, no. 5, pp. 1278-1283, 2017.